Supporting information

Surface Engineering of Perovskites for Rechargeable Zinc-air Battery Application

Maria Christy[a], *Hashikaa Rajan*[a], *Hwawoo Lee* [a], *Iqra Rabani*[c], *Sang Man Koo*[d], *Sung Chul Yi* [a, b,*]

[a]Department of Chemical Engineering, Hanyang University, 222 Wangsimni ro, Seongdong-gu, Seoul 04763, Republic of Korea.

[b]Department of Hydrogen and Fuel cell technology, Hanyang University, 222 Wangsimni-ro, Seongdong-gu, Seoul 04763, Republic of Korea.

[c]Department of Nanotechnology and Advanced Materials Engineering, Sejong University, Seoul 05006, Republic of Korea.

[d]Department of Chemical Engineering, Hanyang University, 222 Wangsimni ro, Seongdong-gu, Seoul 04763, Republic of Korea.

[*]Corresponding author:

Email: scyi@hanyang.ac.kr (Prof. Sung Chul Yi)

Contents

XPS survey and XRD	3
High-resolution XPS Figures	4
FESEM micrographs	5
HRTEM micrographs	6
HRTEM micrographs	7
BET N_2-adsorption desorption isotherms	8
Zinc air battery performance	9
Zinc air battery performance of different composites	10
ORR polarization	11
ORR polarization comparison	12
Chronoamperometry	13
OER polarization comparison	14
ORR and OER polarization	14
ECSA	15
Table 1	16
Table 2	17

Figure S1

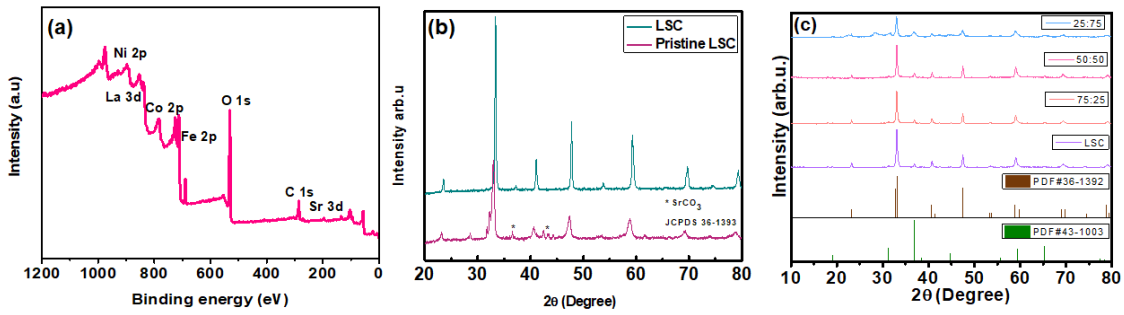

Figure S1. (a) XPS survey of LSC/LDH (75/25); (b) XRD patterns of pristine and LSC prepared by sintering at 1000° and (c) XRD patterns of LSC/LDH (50/50), LSC/LDH (25/75) and LSC/LDH (75/25) with respect to LSC.

Figure S2

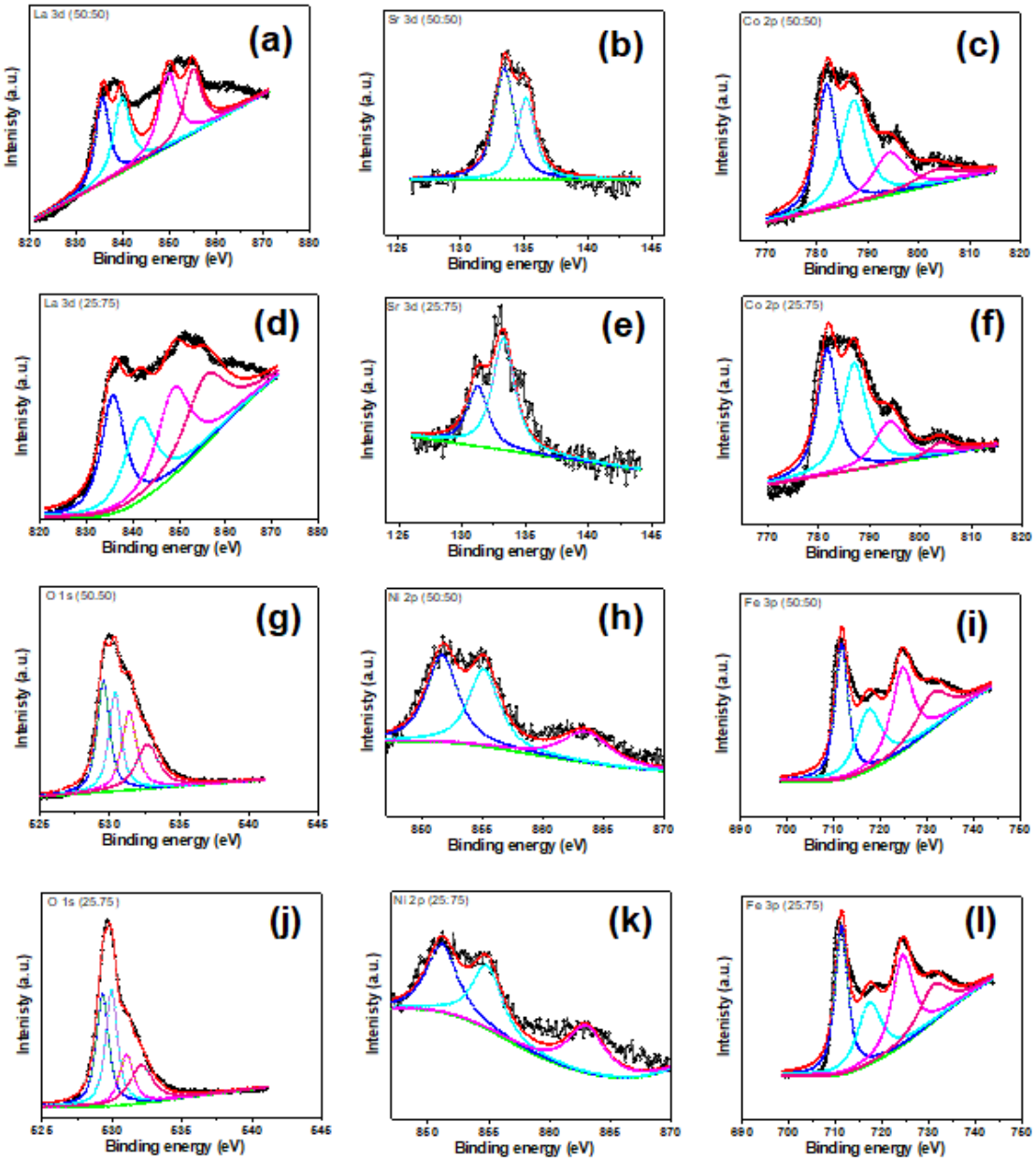

Figure S2. High-resolution deconvolution peaks of (a-f) LSC/LDH (50/50) and (g-l) LSC/LDH (25/75) from XPS measurement.

Figure S3

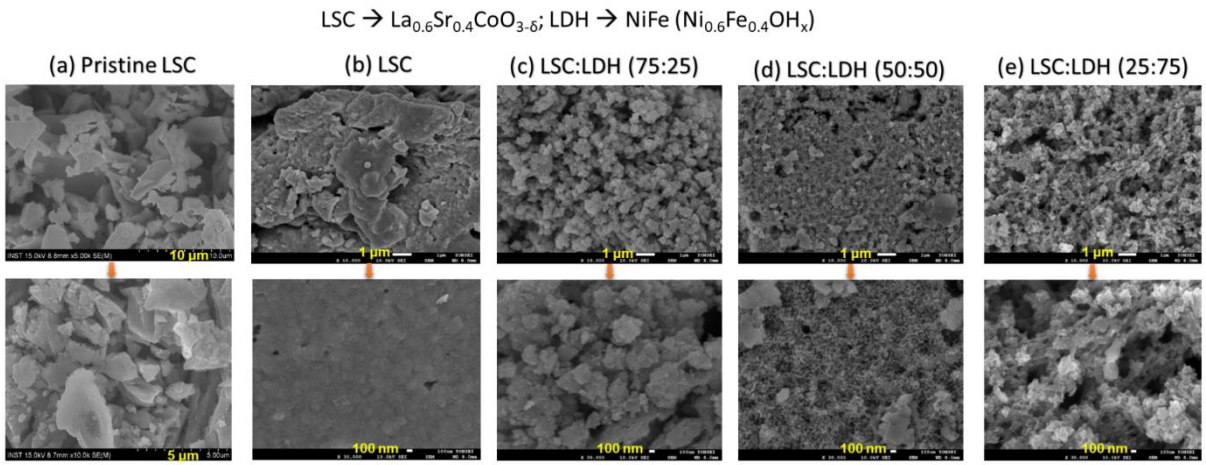

Figure S3. FESEM micrographs of (a) as-synthesized pristine LSC; (b) LSC; (c) LSC/LDH (75/25), (d) LSC/LDH (50/50) and (e) LSC/LDH (25/75) at different magnifications.

Figure S4

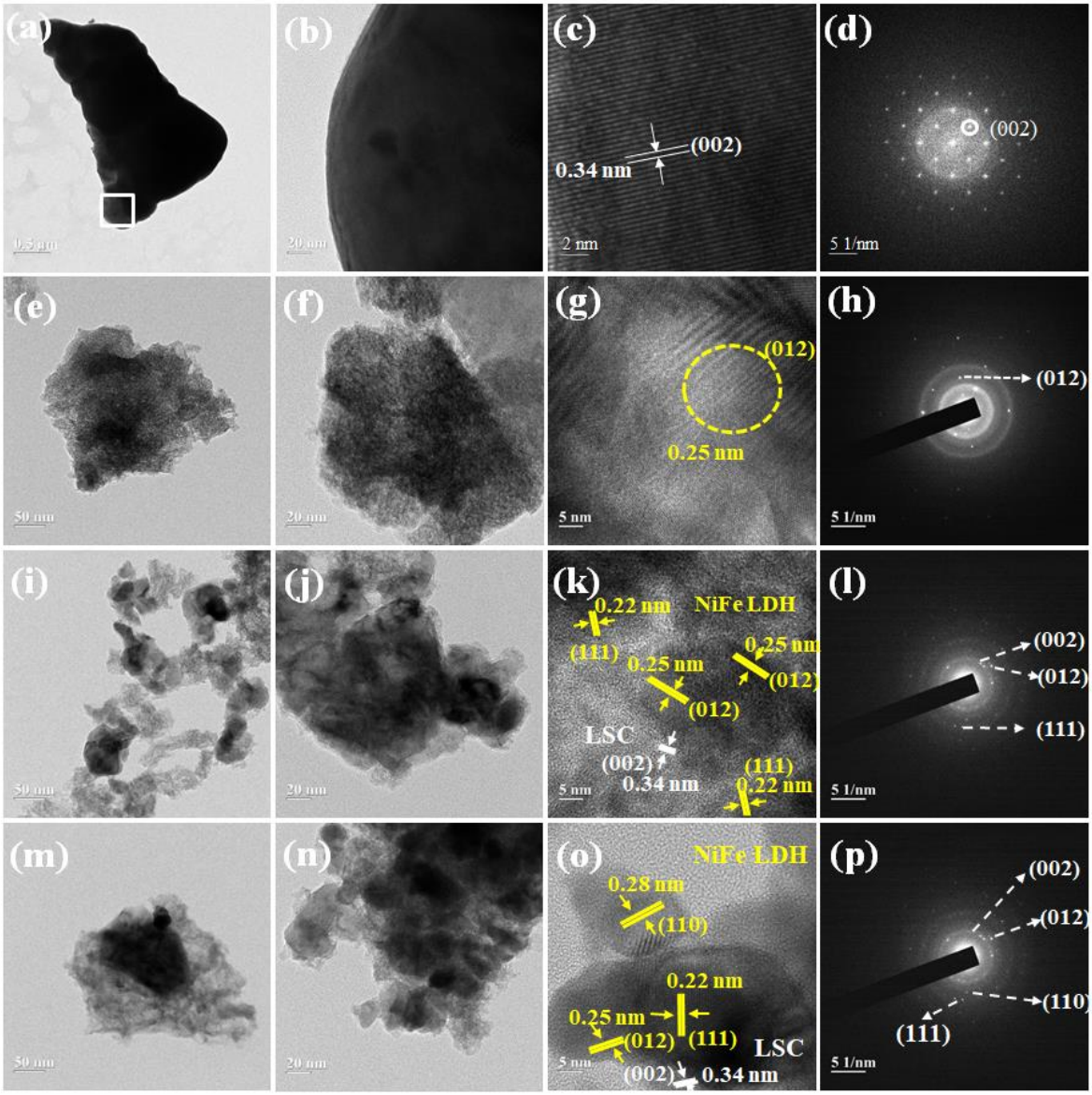

Figure S4. HREM micrographs of (a-d) LSC; (e-h) LSC/LDH (75/25), (i-l) LSC/LDH (50/50) and (m-p) LSC/LDH (25/75) and the corresponding SAED pattern.

Figure S5

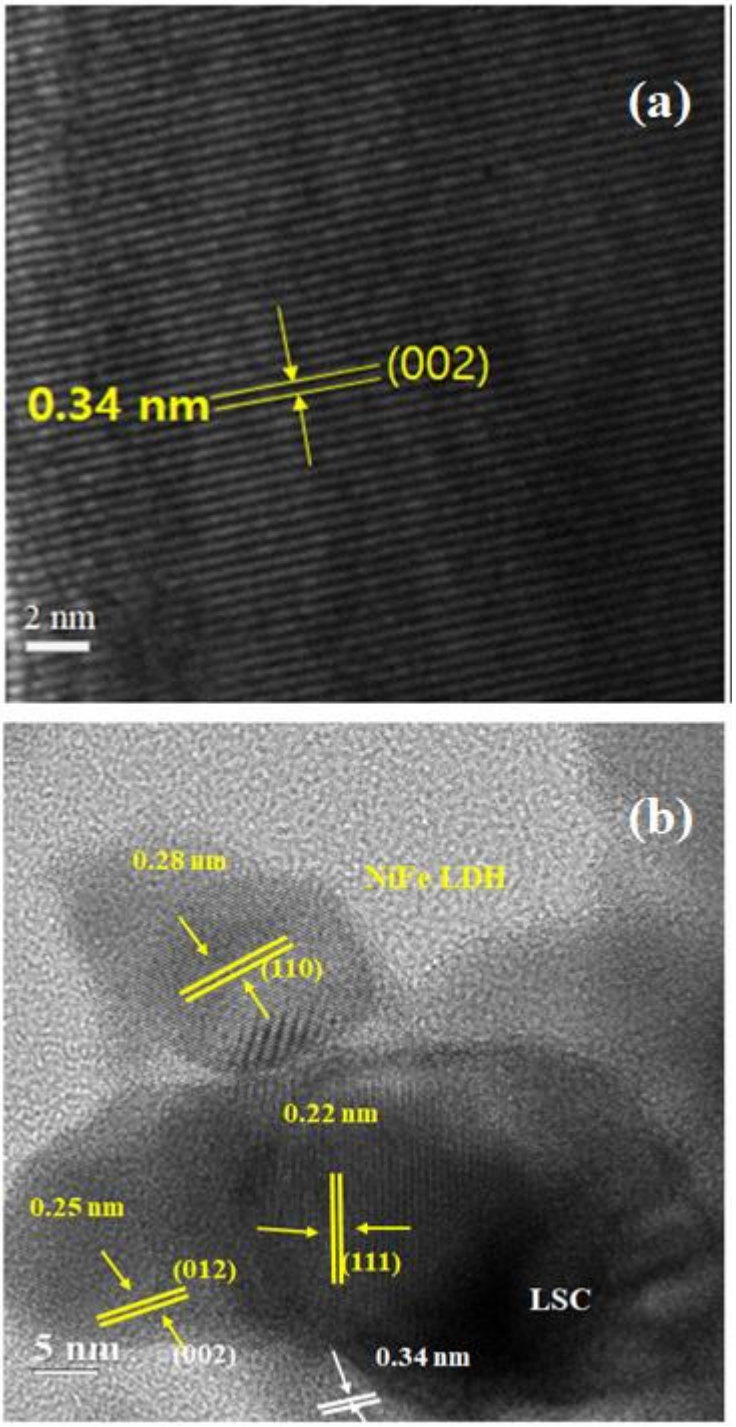

Figure S5. High resolution TEM micrographs of (a) LSC and (b) LSC/LDH (25/75) composite.

Figure S6

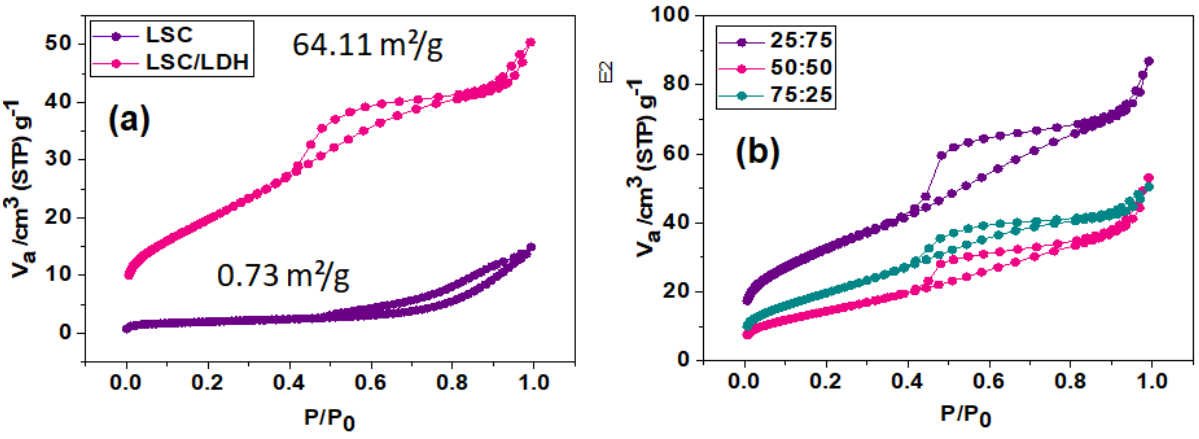

Table S1

Perovskite composition	BET Surface Area m²/g	Pore Size Å	Pore Volume cm³/g
25	107.4411	28.548	0.112817
50	47.4280	33.193	0.058208
75	64.1168	27.810	0.067206

Figure S6. BET N_2-adsorption desorption isotherms of (a) LSC and LSC/LDH (75/25); (b) LSC/LDH (75/25); LSC/LDH (50/50) and (c) LSC/LDH (25/75), comparatively; inset Table S1. Surface properties deduced from BET isotherms.

Figure S7

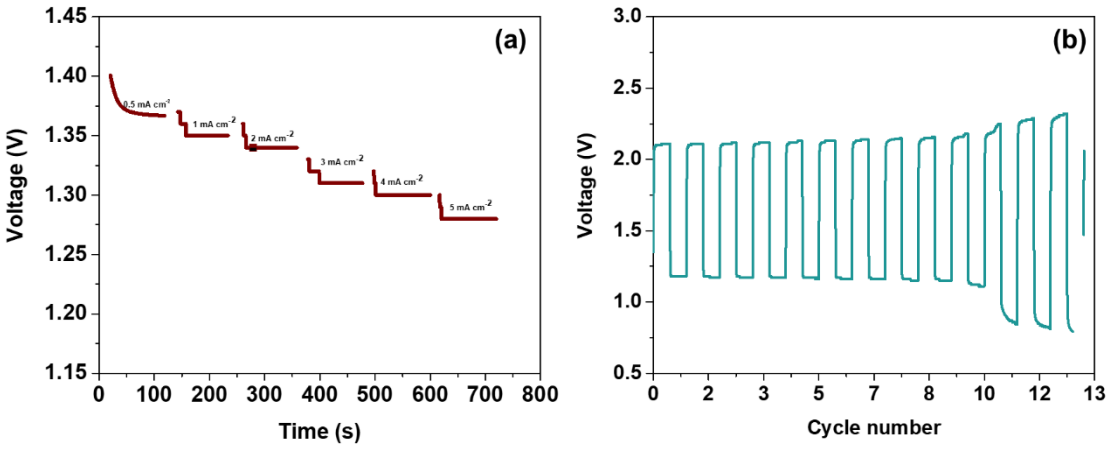

Figure S7. (a) Discharge rate capability of LSC/LDH (75/25) measured at different current densities; (b) Zinc air battery performance of pristine LSC measured at a constant current density of 5 mA cm^{-2}.

Figure S8

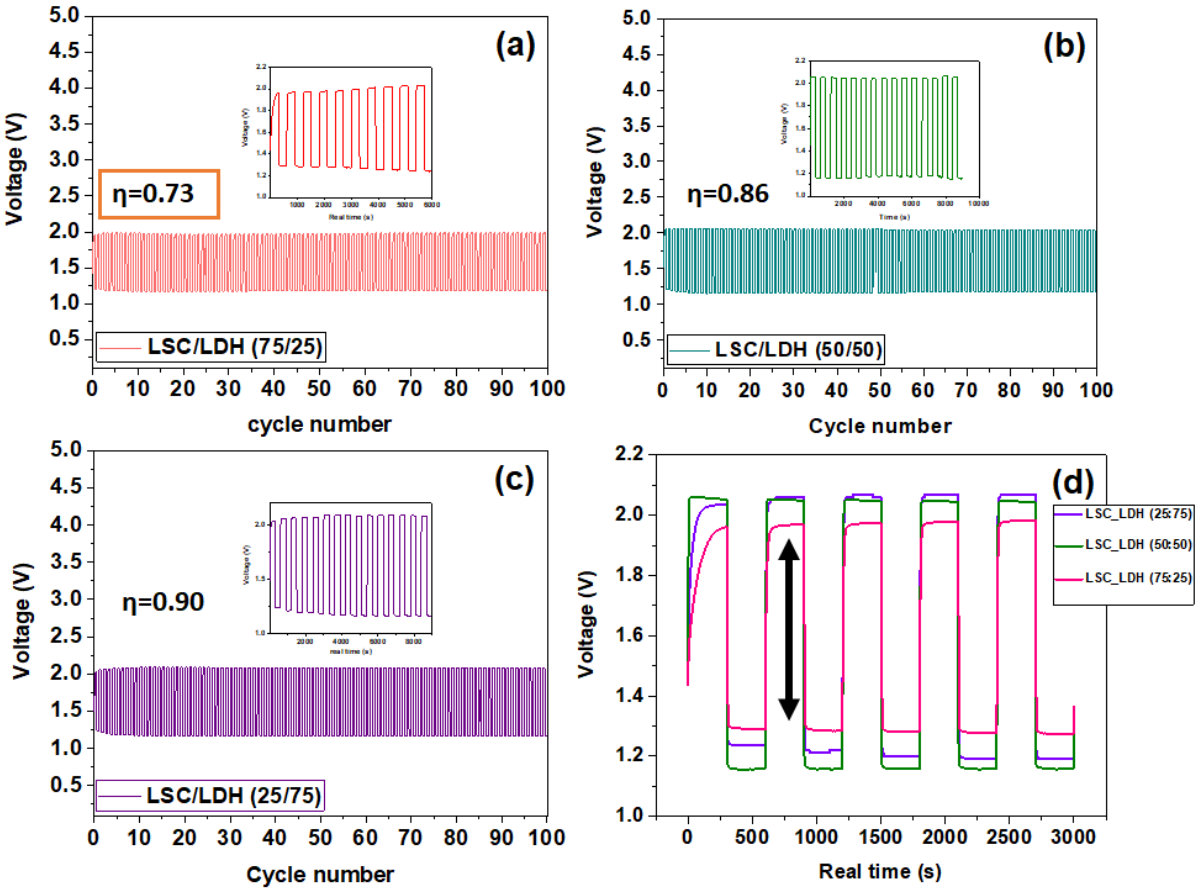

Figure S8. Zinc air battery performance measured at a constant current density of 5 mA cm^{-2} of (a) LSC/LDH (75/25); (b) LSC/LDH (50/50) and (c) LSC/LDH (25/75); and (d) comparison of first few cycles of (a-c).

Figure S9

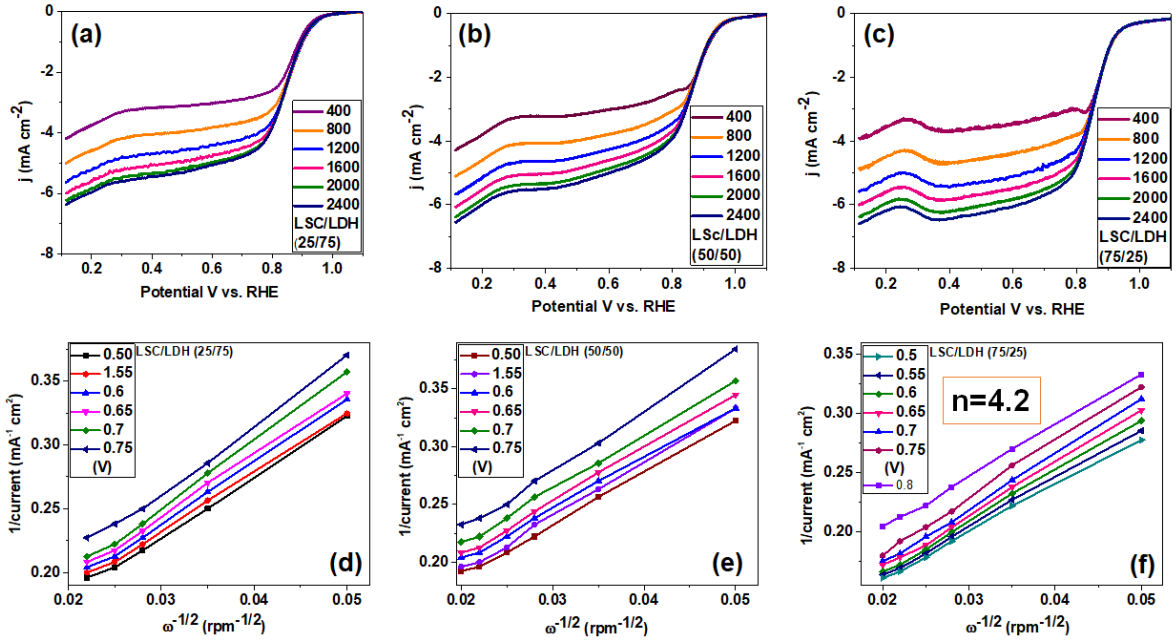

Figure S9. (a-c) The ORR polarization of (a) LSC/LDH (75/25); (b) LSC/LDH (50/50) and (c) LSC/LDH (25/75) measured by varying the rotation speed (400 to 2400 rpm); (d-f) corresponding Koutecky–Levich (K-L) plot of (a) LSC/LDH (75/25); (b) LSC/LDH (50/50) and (c) LSC/LDH (25/75).

Figure S10

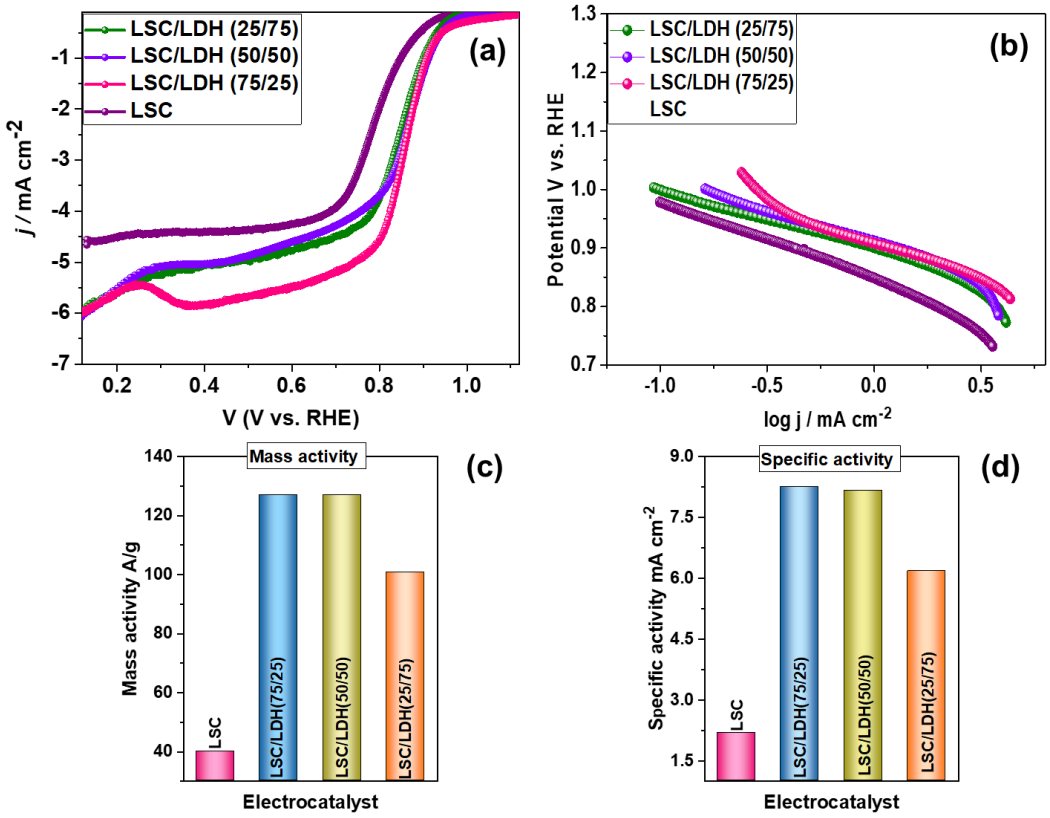

Figure S10. The ORR polarization of (a) LSC/LDH (75/25); (b) LSC/LDH (50/50) and (c) LSC/LDH (25/75) comparatively; (b) Tafel slope values obtained from (a); (c, d) mass activity (MA) A g^{-1} and specific activity (SA) mA cm^{-2} calculated from (a).

Figure S11

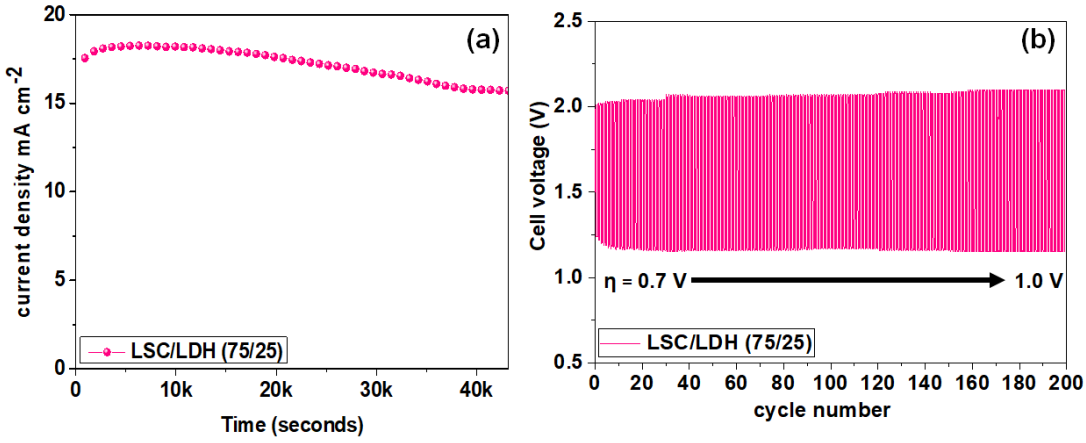

Figure S11. (a) Chronoamperometric durability test of LSC/LDH (75/25) recorded at 10 mA cm^{-2} for 12 h, (b) Zinc air battery performance of LSC/LDH (75/25) measured at a constant current density of 5 mA cm^{-2} for 200 cycles.

Figure S12

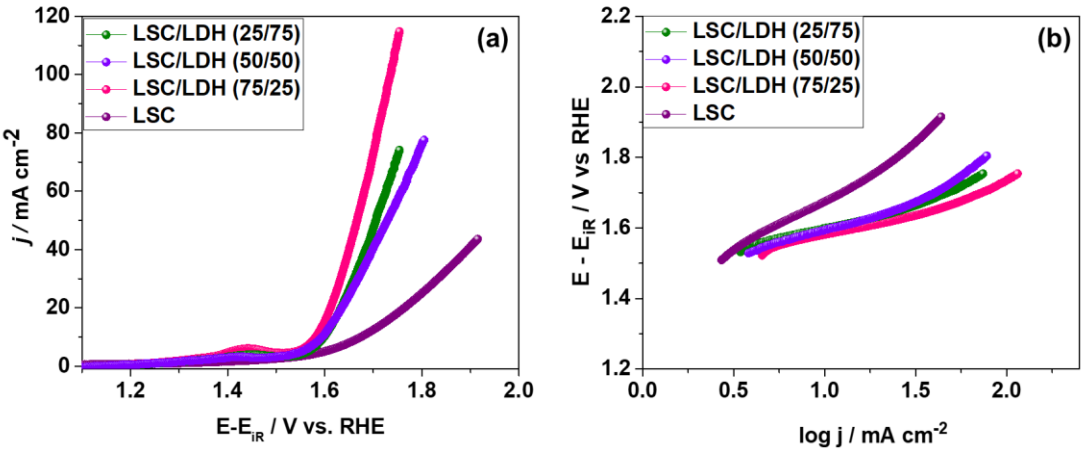

Figure S12. The OER polarization of (a) LSC/LDH (75/25), LSC/LDH (50/50) and LSC/LDH (25/75) in comparison to LSC; (b) Tafel slope values obtained from (a).

Figure S13

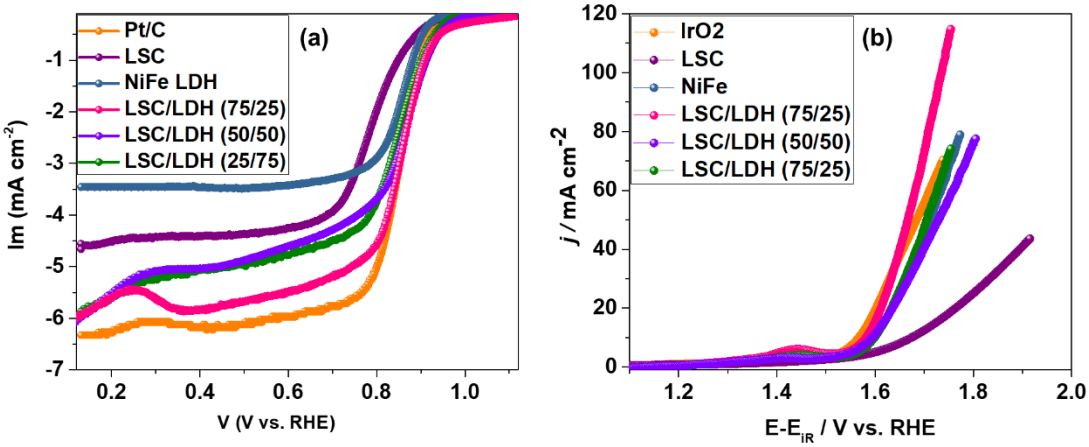

Figure S13. (a) ORR and (b) OER polarization of all the individual material with respect to Pt/C and IrO_2, respectively.

Figure S14

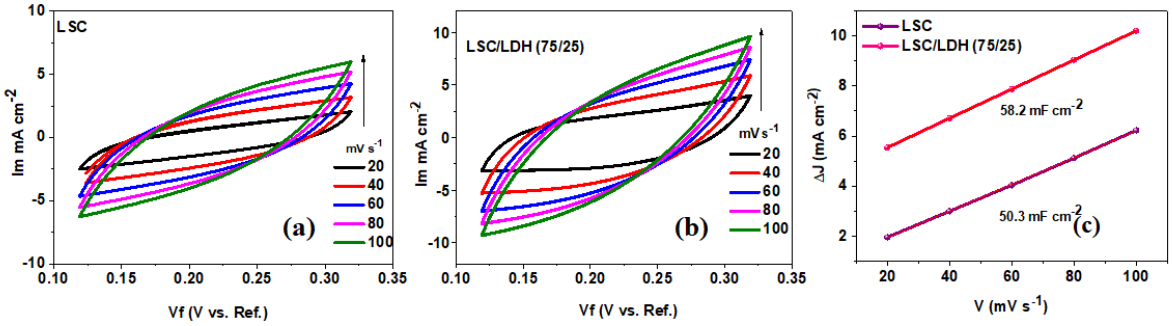

Figure S14. (a, b) CV cycles recorded at different scan rates and (c) the calculated ECSA of OER catalysts from (a) LSC and (b) LSC/LDH (75/25).

Table S1 XPS parameters of LSC and LSC/LDH (75/25)

Name		**Binding energy eV**	**Name**		**Binding energy eV**
La3d	3d5/2	833.32	La3d	3d5/2	835.2
	3d3/2	837.2		3d3/2	851
		849.8			
		854			
Sr3d	3d5/2	132.95	Sr3d	3d5/2	133.4
	3d3/2	134.4		3d3/2	135.1
Co2p	2p3/2	778.54	Co2p	2p3/2	780.65
Co^{3+}, Co^{2+}	2p1/2	794.1	Co^{3+}, Co^{2+}	2p1/2	796.1
O1s	1s lattice	528.61	O1s	1s adsorbed	530
	1s adsorbed	530.6			531.23
			Ni2p	2p3/2	852
			Ni^{2+}		855.5
			Fe2p	2p3/2	712.8
			Fe^{2+}		725

Table S2 Zn–air battery Performance of featuring perovskite oxide-based air cathodes

Electrocatalysts	Application	Overpotential	References
CMO/S Catalyst	Zinc-air battery @5 mA cm^{-2}	0.67	Adv. Energy Mater. 2018, 8, 1800612
Pt-SCFP/C-12	Zinc-air battery @5 mA cm^{-2}	0.77	Adv. Energy Mater. 2020, 10, 1903271
$MnO_2/La_{0.7}Sr_{0.3}MnO_3$	Zinc-air battery @10 mA cm^{-2}	0.79	ACS Appl. Mater. Interfaces 2019, 11, 25870−25881
LSMF	Zinc-air battery @5 mA cm^{-2}	0.8	Applied Energy 251 (2019) 113406
$NdBa_{0.5}Sr_{0.5}Co_{1.5}Fe_{0.5}O_{5+\delta}$	Zinc-air battery @1 mA cm^{-2}	0.7	J. Mater. Chem. A, 2019,7, 24231-24238
PBSCN1	Zinc-air battery @1 mA cm^{-2}	~0.8	ChemElectroChem 2019, 6, 3154 –3159
LMCO	Zinc-air battery	0.8	Inorg. Chem. 2019, 58, 12, 8208–8214
BSCF/NiFe	Zinc-air battery @5 mA cm^{-2}	0.89	ACS Appl. Mater. Interfaces 2019, 11, 39
$PrBa_{0.5}Sr_{0.5}Co_{2-x}Fe_xO_{5+\delta}$	Zinc-air battery @10 mA cm^{-2}	0.8	ACS Nano 2017, 11, 11, 11594–11601
$La_{0.7}$50nm	Zinc-air battery @10 mA cm^{-2}	0.75	Energy Environ. Sci., 2016,9, 176-183
LSC/LDH (NiFe)	Zinc-air battery @5 mA cm^{-2}	0.73	This work